

Capability of Tokai strainmeter network to detect and locate a slow slip

K. Z. Nanjo^{1,2,3,*}

¹ Global Center for Asian and Regional Research, University of Shizuoka, 3-6-1, Takajo, Aoi-Ku, Shizuoka, 420-0839, Japan

² Center for Integrated Research and Education of Natural Hazards, Shizuoka University, 836, Oya, Suruga-Ku, Shizuoka, 422-8529, Japan

³ The Institute of Statistical Mathematics, 10-3, Midori-cho, Tachikawa, Tokyo 190-8562, Japan

* Correspondence: nanjo@u-shizuoka-ken.ac.jp; Tel.: +81-54-245-5600

Received: date; Accepted: date; Published: date

Abstract: The Tokai Strainmeter Network (TSN), a dense network deployed in the Tokai region, an easternmost region of the Nankai trough, monitors slow slips considered to reflect changes in the coupling state of the plate boundary. As was seen for the 2011 Tohoku-oki earthquake of magnitude (M) 9, slow-slip propagation may trigger a large earthquake, so it is desirable to monitor slow slips from when they are small. It is important to evaluate the current capability of TSN to detect and locate slow slips. For this purpose, we modified the probability-based magnitude of completeness developed for seismic networks to be applicable to the evaluation of TSN's performance. We show that TSN is capable of detecting and locating an $M5$ -class slow slip in and around the TSN. A comparison with previous studies on precursory slow slips implies that TSN can monitor a slow slip before it reaches the final size ($M6+$) when the eventual Nankai trough earthquake occurs if such slip occurs in and around the TSN. We explore a possible use of our method to assess the network's performance for cases where virtual stations are added to the existing network. We propose the use of this application when devising a strategic plan of the TSN to extend its coverage to the entire eastern half of the Nankai trough, which historically tends to rupture first.

Keywords: Crustal deformation; Earthquake location; Earthquake prediction; Fault slip; Plate boundary; Seismicity; Statistical methods

1. Introduction

More than 70 years have passed since the last series of Nankai trough earthquakes, the 1944 Tonankai earthquake and the 1946 Nankai earthquake, both belonging to a magnitude (M) 8 class. The possibility of large earthquakes in the entire Nankai trough has now increased. The Japan Meteorological Agency (JMA), in collaboration with many institutions and universities, monitors seismicity and crustal deformation of the Nankai trough 24 hours a day [1]. Dense networks of instruments accumulate a continuous stream of data related to seismicity, strain, crustal movement, tilt, tidal variations, ground water fluctuations, and other variables. Among them is the strainmeter network in the Tokai region, hereafter referred to as the Tokai Strainmeter Network (TSN), which is operated by JMA (Figure 1).

The main task of the TSN is to monitor changes in the coupling state of the plate boundary by detecting and locating slow slips. Slow slips that grow over time may result in large earthquakes, as was observed for the 2011 $M9$ Tohoku-oki earthquake [2]. Thus, it is necessary to detect and locate slow slips when they are still small. In this study, we estimated the capability of TSN to detect and locate a small slow slip.

Our approach is based on the Probabilistic Magnitude of Completeness (PMC) method that has been developed for seismic networks (e.g., [3-5]). This study is the first to be applied to a strainmeter network. This PMC-based method relies on empirical data. Based on this data, we first derive station probability for each station (P_{st}), which is the probability that the station was used to detect and locate a slow slip of a given M at a given distance from the station (L). From the P_{st} for all stations, we obtain the probability (P_{dl}) of detecting and locating slow slips of M at a point (x) for three or more stations. If we apply this method to TSN, the product is a map of P_{dl} for M . We foresee a feedback for JMA network operators by providing a tool to infer spatial heterogeneity of current monitoring ability. This tool will be used as a basis to help future planning for optimizing network coverage.

JMA, with a similar motivation as that shown in this study, mapped the lower-limit magnitude (M_{LL}) to detect and locate slow slips in the Nankai trough [6]. In this mapping, it calculated crustal deformation due to a slow slip of given M at x on the plate interface, using the method of internal deformation due to shear fault in an elastic half-space [7]. A criterion for each station was set such that the synthesized signal-to-noise ratio was a predefined value such as 2 or 3 [8]. If a slow slip of M at x caused elastic strain changes that satisfied the criterion at three or more stations, then the slow slip was considered to have been detected and located. For each x , the minimum magnitude to satisfy the criterion is searched, and this magnitude is mapped as M_{LL} at x . However, it is nontrivial to assign the noise level for each station because tidal correction [9,10], geomagnetic correction (multicomponent strainmeters) [11], and precipitation correction (volumetric strainmeters) [12] are conducted as pre-processes to remove noise for each analysis. These noises vary with time and location [8]. Moreover, setting the synthesized signal-to-noise ratio is completely arbitrary when calculating M_{LL} .

Although both methods are based on different ideas and approaches, the results we obtained show general agreement with JMA's results. Moreover, the results of both methods show that TSN is capable of detecting and locating $M5$ -class slow slips in and around the network. This suggests that it is possible to avoid missing a slow slip before it reaches its final size ($M6-6.5$) [13] leading up to an eventual Nankai trough earthquake that starts in and around TSN.

2. Methods

The PMC-based method relies on two sources of data: (1) station data describing the location for each station in the network; (2) the slow-slip catalogue describing the location, time, and M for each slow slip including data describing which stations were used to detect and locate each event (see [3-5]). The method is divided into an analysis part and a synthesis part. In the analysis, data triplets are first compiled for each station. A triplet contains, for each slow slip, (i) information on whether or not this station was used for detecting and locating the event, (ii) the M of the event, and (iii) its distance L from the station.

Using triplets for each station, we want to determine station probability $P_{st}(M, L)$, the probability that the station detects changes in strain associated with a slow slip for a given set of M and L to locate the events. As described later, the number of slow slips used for analysis is 35, which is not enough to reliably estimate $P_{st}(M, L)$ for individual stations. For a more reliable estimate, we used the idea of Bachmann et al. [14] in which data triplets from all stations that have been used at least once for the period of interest are stacked (Figure 2a) to compute $P_{st}(M, L)$ (Figure 2b). We smoothed $P_{st}(M, L)$ by applying simple constrains: (1) detection probabilities cannot decrease for large magnitudes at the same distance and (2) detection probabilities cannot decrease with smaller distances for the same magnitude (e.g., [3-5]). This smoothing accounts for high probabilities at short distances and large magnitudes in Figure 2c.

One problem arises for stations that have never been used for event detection and location even though these stations were in operation. We realize that they were relatively far from the slow slips during the observed period (2012-2016) in Figure 1, assuming that JMA only uses these stations if slow slips occur near them. We assigned $P_{st}(M, L)$ for all stations in operation, regardless of whether or not they have been used for event detection and location.

In the synthesis part, basic combinatorics was used to obtain detection-location probabilities $P_{dl}(M, x)$ for detecting and locating a slow-slip of M at x (Figures 3a and 3b), given a specific network configuration. For TSN, $P_{dl}(M, x)$ is the probability that three or more stations detect changes in strain associated with a slow slip with M to locate the event at x [6,13]. This minimum number of stations must be adjusted if the condition of the TSN is based on another number of stations.

2. Data

JMA is recording short-term slow slips in the Tokai region with the TSN, one of the densest networks in Japan, operating 11 multicomponent strainmeter stations and 16 volumetric strainmeter stations (Figure 1). The former strainmeters are generally buried at depths of 400-800 m, while the latter ones in the range of 150-250 m. The station list can be obtained from JMA.

Short-term slow slips in the Tokai region release energy over a period of a few days to a week, rather than seconds to minutes which is characteristic of a typical earthquake. Long-term slow slips that slip over a period of a few months to several years were recorded by GNSS. In the Tokai region, long-term slow slips of $M7.0$ and $M6.8$ occurred in 2001-2005 and 2013-2017, respectively. Short-term slow slips can be seen at depths of 30-40 km, and the down-dip side of the long-term slow slips is at a depth of 20-30 km. We are interested in the capability of TSN to detect and locate small slow slips. We used the slow-slip catalogue [15], which includes 35 events having moment magnitude $M5.1$ - 5.8 with depths 26-41 km from 2012 to 2016 in the Tokai region. Based on the slow-slip catalog and the list of strainmeter stations, we compile data triplets.

To compute $P_{st}(M, L)$ in Figure 2, we use data triplets with a magnitude and distance close to a given pair (M, L) . We selected triplets by measuring the distance between each triplet and the pair (M, L) . To measure such a distance, we needed to define a metric in the magnitude-distance space. Schorlemmer and Woessner [3] proposed the use of an attenuation equation for magnitude-based determination of earthquakes located in a given local seismic network. In this study, we followed this idea and used the attenuation equation used by JMA [5,16]. The magnitude of a slow slip is defined by the moment magnitude M , and not by the JMA magnitude (M_{JMA}). However, when the moment magnitude exceeds $M = 5$, M_{JMA} can be considered statistically equivalent to M , while below $M = 5$, M_{JMA} is smaller than M [17,18]. The slow slips we analyzed had an $M > 5$. Thus, we assumed that the attenuation equation used by JMA is directly applicable to define a metric in the magnitude-distance space for our case.

Our approach assumes that single slow slips occur at different times because multiple slow slips that occurred at different locations at the same time were not reported by JMA during 2012-2016.

4. Results

4.1. Sensitivity checks on dependence of volumetric and multicomponent strainmeters on station probability

We first performed simple sensitivity checks on dependence of four different azimuths of multicomponent strainmeters of a station on P_{st} . Although data were sparse, we separately considered P_{st} for each of the four azimuths. Figure 3 shows an example from station “Tahara Takamatsu”. Generally, the patterns are similar to each other. This is due to the fact that for most cases, strain changes for all four components were used to detect and locate slow slips. The same feature was seen for another station “Urugi Iwakura” (Figure 4). We observed the same trend for other multicomponent stations. Thus, for each multicomponent strainmeter station, we stacked triplets from the four components and define these as data triplets of that station.

A similar sensitivity analysis was performed for dependence of volumetric and multicomponent strainmeters on P_{st} . We selected “Tahara Fukue” (volumetric strainmeter station) and “Tahara Takamatsu” (multicomponent strainmeter station), spatially close to each other (Figure 5). The former measures volumetric change while the latter measures changes in diameter (line strain) of the four azimuths. Generally, the patterns were very similar to each other. We treated all stations equally regardless of whether strainmeters were volumetric or multicomponent in nature.

4.2. Mapping probabilities

Figure 6 shows the spatial distribution of P_{dl} for $M = 5.1$ and 5.8 (the minimum and maximum magnitudes of observed slow slips, respectively). We used a grid spacing of $0.05^\circ \times 0.05^\circ$ and computed P_{dl} at the plate boundary interface [19–22]. As expected, P_{dl} increased with M . Figures 6 and S1 show that slow slips during 2012–2016 are located in areas with predominantly high probabilities, showing consistency between our synthesis and the observation. If $P_{dl} \geq 0.9999$ is considered as an indication that a slow slip will not be missed [4], the maps in Figures 6 and S1 indicate that in and around TSN, $M5$ -class slow slips can be detected and located. P_{dl} in offshore regions is expectedly lower than within the network: P_{dl} gradually decreases with distance from the coast. This is because no station is in operation in offshore regions. The anticipated source zone of the Tokai earthquake, the Tokai segment in the Nankai trough, is not covered by a region of $P_{dl} \geq 0.9999$ for $M = 5.1$ – 5.8 (Figure 6 and S1). A slow slip with $M \leq 5.8$ would likely be missed at the southernmost tip of the anticipated source zone.

To support the method validation, we further showed consistency between our synthesis and the observation by creating maps of P_{dl} based on P_{st} computed for each of the stations that were used to detect and locate slow slips in the 2012–2016 period (Figures S2 and S3), where P_{st} for each multicomponent strainmeter station was derived from stacking all triplets for the four components of the station. Stations that were not used for event detection and location in the same period were not included in the computation of P_{dl} . Note that P_{st} that was computed by the stacked triplets from all stations (Figure 2) is not used. Similar to Figures 6 and S1, we observed consistency between our synthesis and the observation in Figure S3.

Among all stations in TSN, three showed a station characteristic in which the occurrence frequency of irregular changes in the strain was high [8]. We created the same maps in Figure 6 for the case that these stations were excluded from the P_{dl} computation (Figure S4), showing that general patterns do not vary between the two in Figures 6 and S4.

4.3. Virtual installation of stations

To infer the effect of adding station(s) to the TSN on P_{dl} , we performed scenario computations by virtually placing additional stations to the network configuration. A fundamental problem is the definition of P_{st} that is used for individual stations installed for the virtual case. Such P_{st} depends on station characteristics, local site, and noise conditions. We are interested in cases where additional submarine stations are virtually placed in offshore regions. Two seafloor strainmeter stations under DONET (Dense Oceanfloor Network system for Earthquakes and Tsunamis), not involved in TSN, are operating in a far-offshore region from the Kii Peninsula near the trough axis (33.0 – 33.5°N , 136.0 – 136.5°E) [23]. As an approximation, we assumed that P_{st} for a virtual seafloor station was the same as that used for an inland station in Figure 2. We argue that this is a best-case scenario because this purpose is not to discuss the detailed pattern of P_{dl} for virtual cases, but to infer the network performance as a rule of thumb with low costs. However, we are aware that the seafloor station characteristic may be very different from the characteristic for inland stations because of local site conditions, and that for appropriate station planning additional geological data are necessary.

Figure 7 shows the maps of P_{dl} for $M = 5.8$ for virtual station installations at different locations in addition to the existing network. The first two frames (a,b) show examples of the installation of single stations where we assume this installation on the rims of the continental shelf. In the third frame (c), it is assumed that one station is installed in a far-offshore region. Comparison with the map in Figure 6b shows that the installation of single stations improves the detection-location capabilities in offshore regions. However, the effect is limited, as expected.

Figures 7d–f show cases where the number of stations installed at offshore locations are increased. Even if stations are located more sparsely in offshore regions than in inland regions, the detection-location capability of a slow slip is pronouncedly enhanced. The difference between single station installation (Figures 7a–c) and multiple station installation (Figures 7d–f) is clear. As in section

4.2, we compared the anticipated source zone of the Tokai earthquake and a region of $P_{dl} \geq 0.9999$. A slow slip with $M \geq 5.8$ would likely not be missed in the zone, given the configuration in Figure 7f. This type of scenario computation has already been performed for seismic networks, and shows a similar effect [3,4].

4.4. Comparison between the present and previous studies

A conventional assessment of M_{LL} has been applied to the entire Nankai Trough [6] by using model assumptions that the medium is elastic and the strainmeters record elastic strain changes caused by slow slips [7]. We addressed a fundamental question if our PMC-based method and the conventional method provided similar results.

The map of M_{LL} for the Nankai trough was created based on the TSN operated by JMA and the network operated by AIST (National Institute of Advanced Industrial Science and Technology). Since only three AIST stations are in operation in the Tokai region, we assumed that the spatial pattern of M_{LL} based on this hybrid network was comparable to the maps of P_{dl} purely based on TSN.

Figure A1a shows that values of $M_{LL} \leq 5.8$ (green to white) fall in and around the hybrid network in the Tokai region. The probability map of $M = 5.8$ (Figures 6b and A1b), which shows that values of $P_{dl} \geq 0.9999$ fall in and around TSN, suggests consistency with the M_{LL} map. If we take a small threshold magnitude, $M = 5.5$, we again see general agreement between the region of $P_{dl} \geq 0.9999$ (Figure S1e) and the region of $M_{LL} \leq 5.5$ (green in Figure A1a), although detailed differences in patterns demonstrate that the former region spreads wider toward the offshore than the latter region. Regardless of the different approaches used in this study, including a conventional approach, we found that the results were generally similar to each other.

5. Discussion

As an example of a precursor phenomenon just before an earthquake occurs, tilting associated with the 1944 M8-class Tonankai earthquake has been observed [24,25]. A remarkable precursory tilt started two or three days before the earthquake. The precursory amount of change corresponds to about 30% of the amount of change at the time of the earthquake. In contrast, many studies using close-in strainmeters and tiltmeters have concluded that a precursory slip, if any, is very small, $< 1\%$, for many California earthquakes [26,27] such as the 1987 Whittier Narrows earthquake ($M = 6.0$), the 1987 Superstition Hills earthquake ($M = 6.6$), the 1989 Loma Prieta earthquake ($M = 6.9$), and the 1992 Landers earthquake ($M = 7.3$).

Scholz et al. [28] made detailed laboratory measurements on frictional characteristics of granite. In the condition where the stick-slip predominates, the stick-slip is preceded by a small amount of stable slip, which accounts for about 2-5% of the unstable slip that follows. Lorenzetti and Tullis [29] used mechanical models of faulting during an earthquake cycle that was based on the rate- and state-dependent friction law, and predicted that the amount of pre-seismic moment release was $< 0.5\%$ of the earthquake moment for most simulations. Using a simulation of the earthquake cycle in the Tokai region, Kato and Hirasawa [30] did not directly estimate the magnitude of a precursory slow slip. However, their result indicates that its magnitude varies, depending on values given for different parameters. Furthermore, in their earthquake-cycle simulation, it was commonly seen that remarkable abnormal crustal movements started to appear over a wide area several days to several hours before the occurrence of an earthquake.

It is difficult at present to judge the magnitudes of slow slips that are precursory phenomena to the Nankai trough earthquake, but it is necessary to assume a severe situation. While the Nankai trough earthquakes belong to a M8-class or larger, a precursor slip is about 1% of the earthquake: the final precursory slow slip with M6-6.5 is assumed [13]. This study shows that TSN is capable of detecting and locating M5-class slow slips in and around TSN (Figures 6, A1b, and S1), and an independent study obtained a similar result (Figure A1a). Thus, TSN would most likely avoid missing a slow slip before it reaches its final size when the eventual earthquake occurs if the slow slip occurs in and around TSN.

We have not yet considered early detection-location capability of a slow slip. Data obtained by strainmeters under TSN are being watched 24 hours a day at JMA, so that rapid earthquake information is in operation in real-time [1]. Miyaoka and others [8,31] developed a stacking method in which data at different strainmeter stations are added to increase the signal-to-noise ratio for early detection of crustal deformation associated with slow slips. This method, in combination with our PMC-based approach, will lead to more realistic evaluation of TSN's performance regarding early detection-location capability of a slow slip.

The history of the Nankai trough earthquakes shows that the eastern half of this trough tends to rupture first [32–36]. It is desirable to explore the possibility of making a strategic plan to TSN to extend its coverage to the entire eastern half of the Nankai trough, where, except for the Tokai region and a part of the Kii Peninsula, the detection-location capability of a slow slip is currently low [6]. For this purpose, a tool proposed in this study can help network planning with simulation of virtual station installation (Figure 7).

However, we understand that the effectiveness of this tool needs to be investigated in more detail as it is a non-trivial task to assume a station characteristic for a new station, especially for a seafloor strainmeter station. Additional information such as local site conditions and geological parameters need to be available. Nonetheless, as a rule of thumb, the PMC-based method can help, with reduced costs, to estimate network performance and infer locations for future stations.

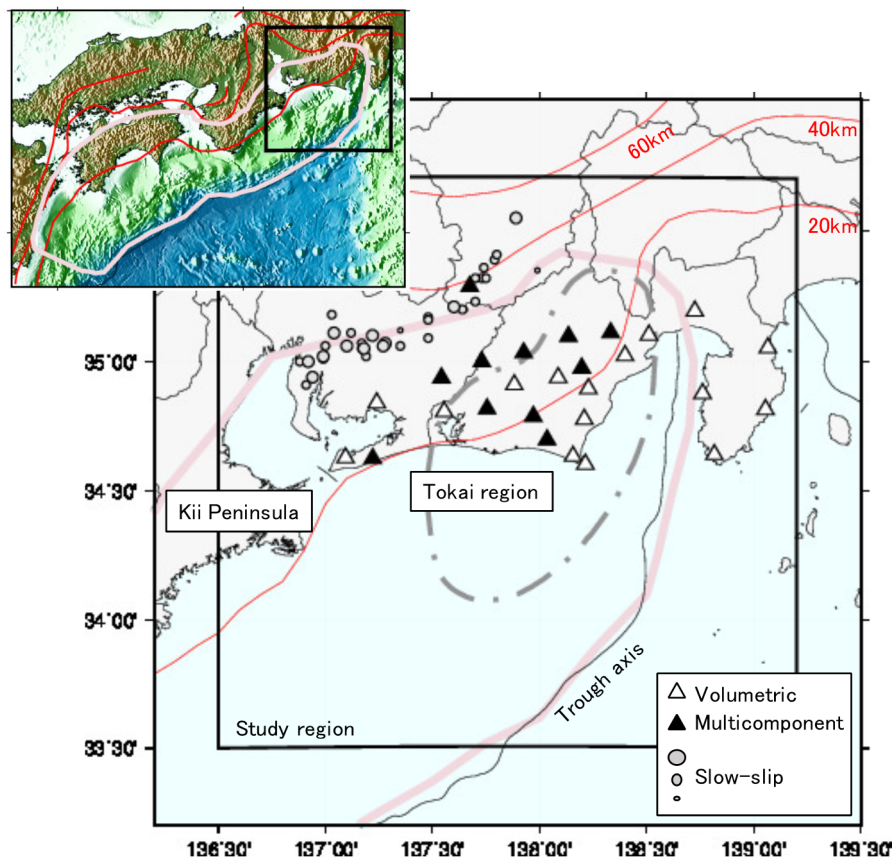


Figure 1. Location map of strainmeter stations (open triangle: volumetric, filled triangle: multicomponent) in the Tokai region. Slow slip (circle): small size, $M \geq 5.1$; middle size, $M \geq 5.4$; large size, $M \geq 5.7$. Chain line: region supposed to be the source of an anticipated Tokai earthquake [37]. Thick purple line: maximum focal region of a megathrust earthquake [37]. Red curves mark depth contour lines [19–22]. Prefectural boundaries are shown by thin black lines. The zoomed-out inset is a map of the Nankai trough, where the study area (black square) is shown.

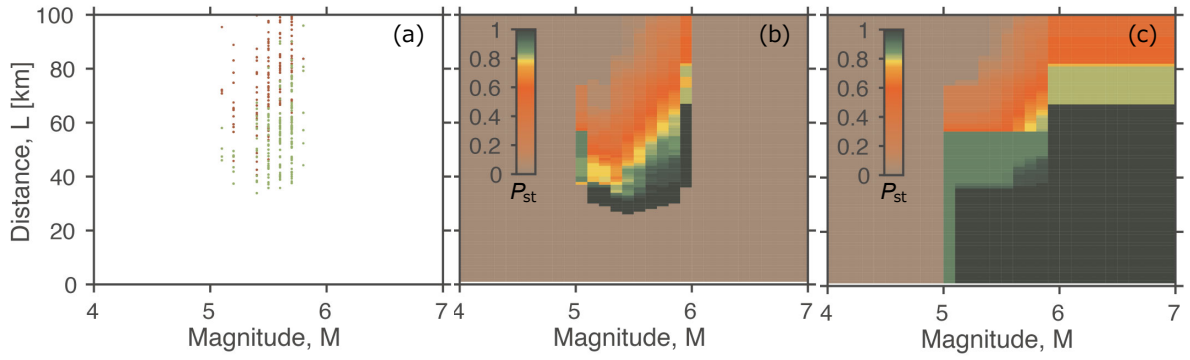


Figure 2. Average station characteristics. (a) Stacked distribution of undetected events (red) and detected events (green) for stations that have been used at least once to record slow slips in 2012-2016. (b) $P_{st}(M, L)$ derived from raw data triplets. (c) Smoothed distribution of $P_{st}(M, L)$. See also Refs. [3-5].

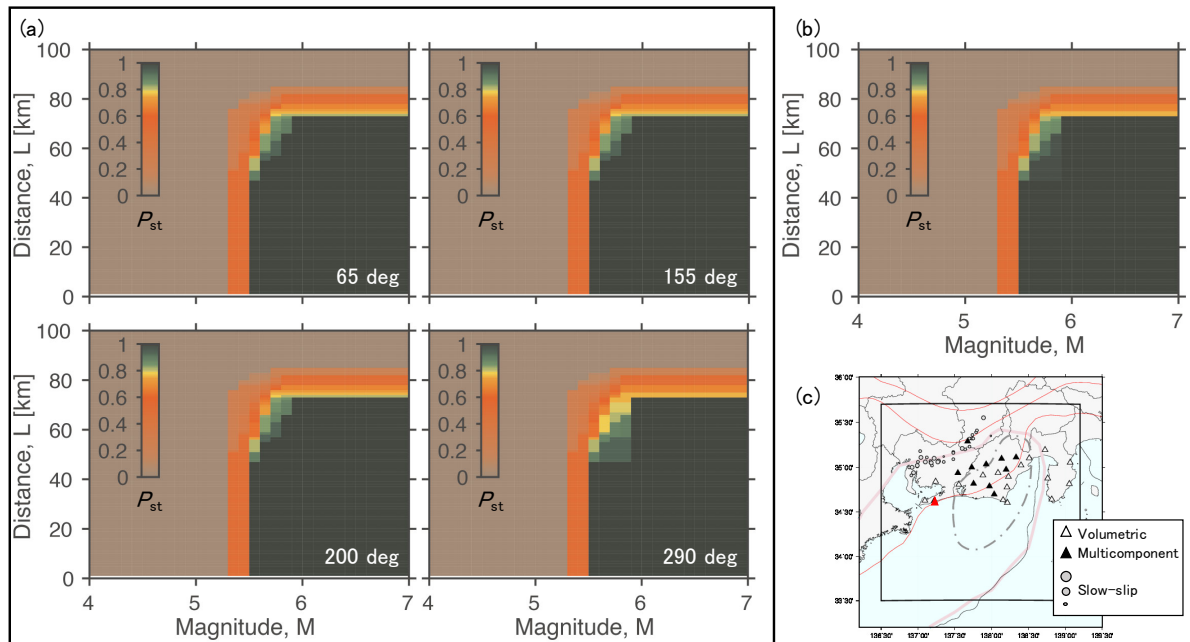


Figure 3. $P_{st}(M, L)$ for four different components with different directions (clockwise from the north) in (a) and average distribution of $P_{st}(M, L)$ over the four components in (b) for station "Tahara Takamatsu", indicated by a red triangle in (c).

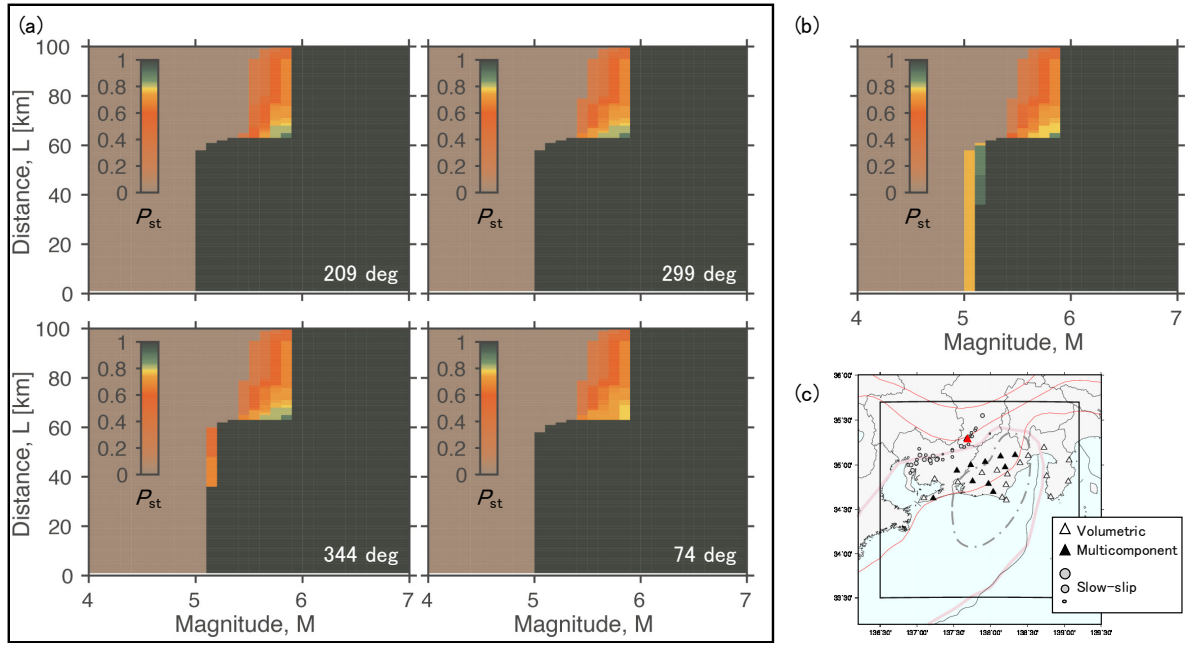


Figure 4. $P_{st}(M, L)$ for four different components with different directions (clockwise from the north) in (a) and average distribution of $P_{st}(M, L)$ over the four components in (b) for station "Urugi Iwakura", indicated by a red triangle in (c).

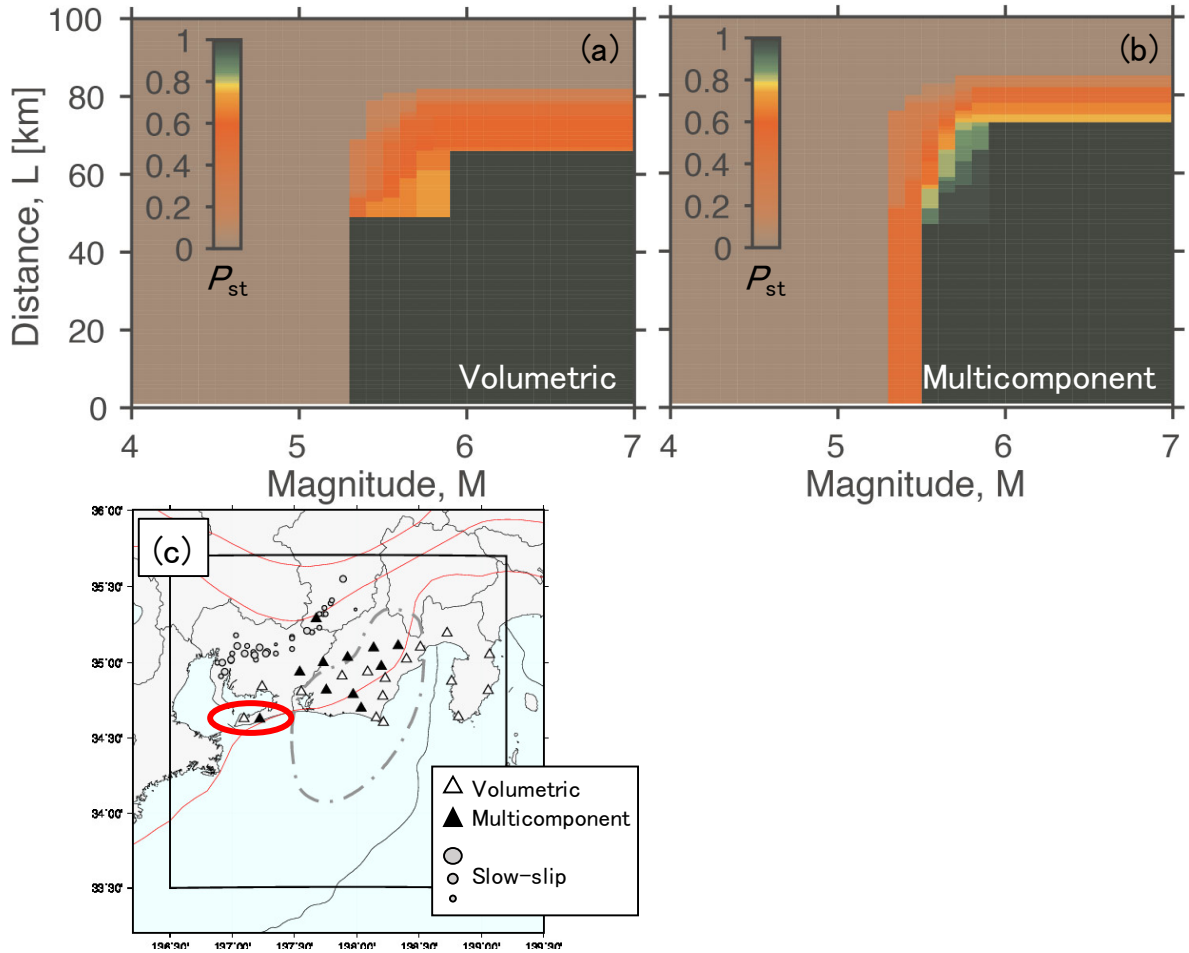


Figure 5. $P_{st}(M, L)$ of strainmeter stations: (a) "Tahara Fukue" (volumetric) and (b) "Tahara Takamatsu" (multicomponent). Locations of the respective stations are indicated by open and filled triangles in the red ellipsoid in (c). $P_{st}(M, L)$ in (b) is the same as that in Figure 3b.

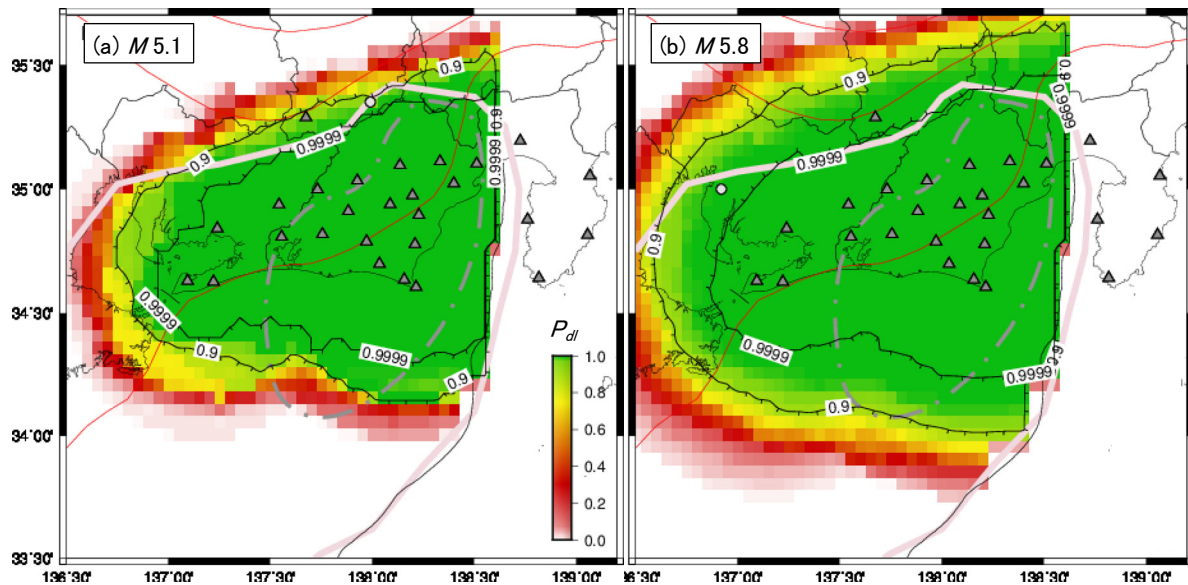


Figure 6. Maps of $P_{dl}(M, x)$ for $M = 5.1$ in (a) and $M = 5.8$ in (b). Stations: triangles. Circles: slow slips of respective magnitude that were recorded in 2012–2016.

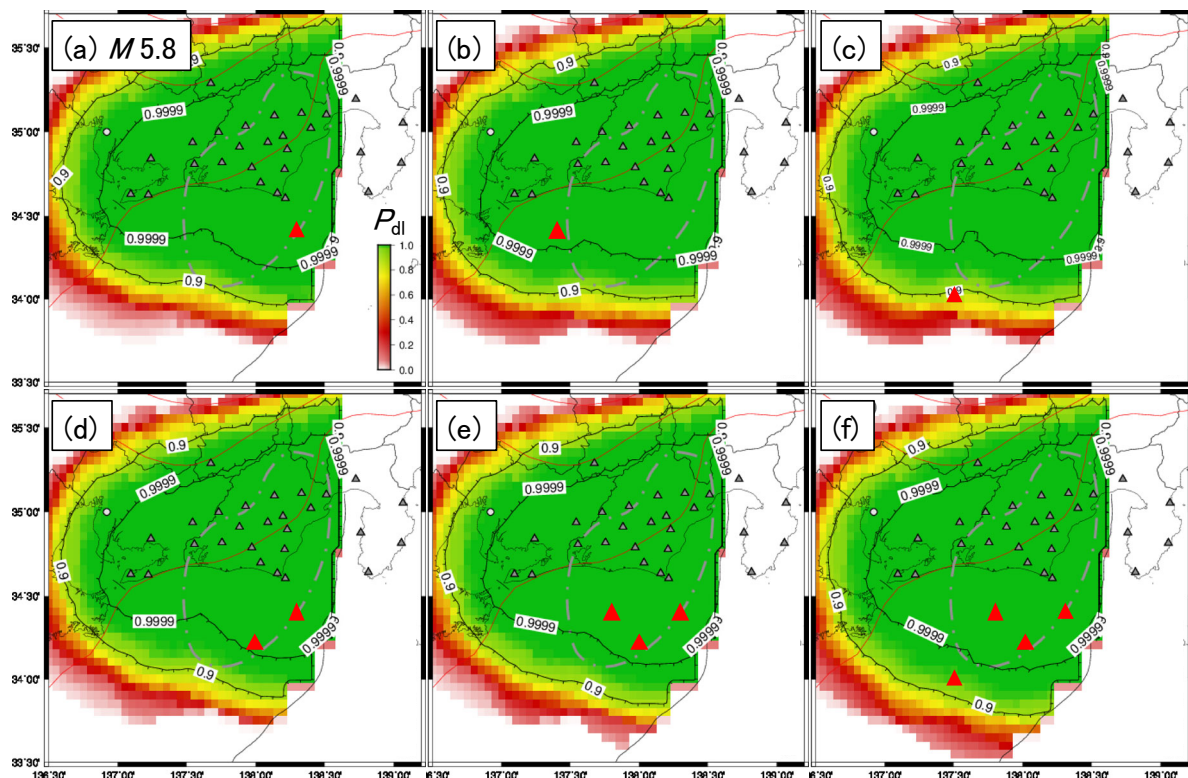


Figure 7. Scenario computation of adding virtual stations (red) to the network (grey). A single virtual station was added to different locations in (a, b, c). (d) We added another station to the configuration (a). We added a third station (e) and a fourth station (f).

Supplementary Materials: The following are available online at www.mdpi.com/xxx/s1, Figure S1: Maps of $P_{dl}(M, x)$ for $M = 5.1$ – 5.8 , Figure S2: $P_{st}(M, L)$ computed for each of the stations that have been used to record slow

slips in 2012–2016, Figure S3: Same as Figure S1, but we used $P_{st}(M, L)$ shown in Figure S2, Figure S4: Same as Figure 6 except that stations where irregular changes in strain frequently occur were not used.

Funding: This work was partially supported by JSPS KAKENHI Grant Number JP 17K18958.

Acknowledgments: The author thanks Y. Ishikawa, J. Kasahara, H. Kimura, and K. Miyaoka for valuable comments. Some figures were produced by using GMT software [38].

Conflicts of Interest: The authors declare no conflict of interest.”

Appendix A

The original of Figure A1a was used by the Working Group on Forecast Ability of Large Earthquakes in the Nankai Trough (September 2016 – July 2017) [39], and is available at [6]. Figure A1 was created by trimming the original figure. M was used in the original, but we replace it with M_{LL} .

The original [6] shows that M_{LL} values vary between 5 and 6.5 in the entire Nankai trough. In the Tokai region, a part of the Kii Peninsula, and a part off Shikoku, we observed $M_{LL} \leq 5.5$. In other regions, M_{LL} was generally between 5.5 and 6.5.

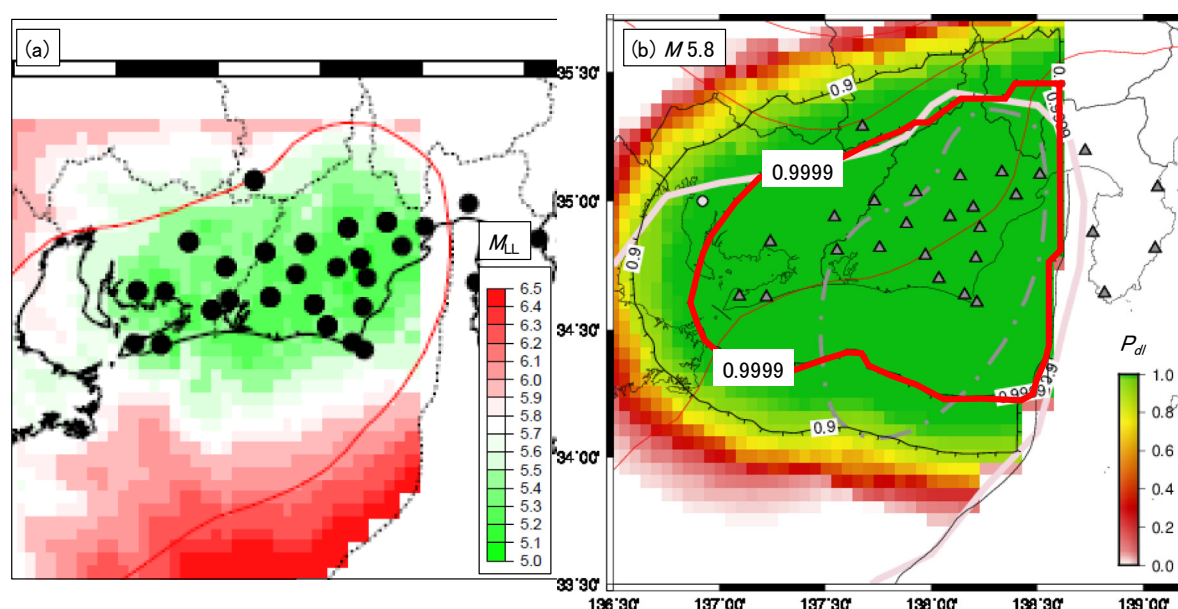


Figure A1. (a) Map of M_{LL} [6]. Circle: strainmeter stations under TSN and those operated by AIST. (b) Same as Figure 6b but the contour line of 0.9999 is highlighted by a thick red line.

References

- Information associated with the Nankai trough earthquakes (in Japanese). <https://www.data.jma.go.jp/svd/eqev/data/nteq/forecastability.html> (accessed on 11 March 2019).
- Kato, A.; Obara, K.; Igarashi, T.; Tsuruoka, H.; Nakagawa, S.; Hirata, N. Propagation of slow slip leading up to the 2011 M_w 9.0 Tohoku-Oki earthquake. *Science* **2012**, *335*, 705–708.
- Schorlemmer, D.; Woessner, J. Probability of detecting an earthquake. *Bull. Seismol. Soc. Am.* **2008**, *98*(5), 2103–2117.
- Nanjo, K.Z.; Schorlemmer, D.; Woessner, J.; Wiemer, S.; Giardini, D. Earthquake detection capability of the Swiss Seismic Network. *Geophys. J. Int.* **2010**, *181*(3), 1713–1724.
- Schorlemmer, D.; Hirata, N.; Ishigaki, Y.; Doi, K.; Nanjo, K.Z.; Tsuruoka, H.; Beutin, T.; Euchner, F. Earthquake detection probabilities in Japan. *Bull. Seismol. Soc. Am.* **2018**, *108*(2), 702–717.
- Monitoring phenomena observed in the Nankai trough and future direction of research and observation (in Japanese). http://www.bousai.go.jp/jishin/nankai/tyosabukai_wg/pdf/h281013shiryoo06.pdf (accessed on 11 March 2019).

7. Okada, Y. Internal deformation due to shear and tensile faults in a half-space. *Bull. Seismol. Soc. Am.* **1992**, *82*(2), 1018-1040.
8. Miyaoka, K.; Yokota, T. Development of stacking method for the detection of crustal deformation - Application to the early detection of slow slip phenomena on the plate boundary in the Tokai region using strain data-. *Zisin (J. Seismol. Soc. Japan, 2nd ser.)* **2012**, *65*, 205-218.
9. Ishiguro, M.; Sato, T.; Tamura, Y.; Ooe, M. Tidal data analysis: an introduction to BAYTAP (in Japanese). *Proc. Inst. Stat. Math.* **1984**, *32*(1), 71-85.
10. Tamura, Y.; Sato, T.; Ooe, M.; Ishiguro, M. A procedure for tidal analysis with a Bayesian information criterion. *Geophys. J. Int.* **1991**, *104*, 507-516.
11. Miyaoka, K. Geomagnetic correction of multi-component strain meters (in Japanese with English abstract). *Quart. J. Seismol.* **2011**, *74*, 29-34.
12. Ishigaki, Y. Precise corrections and detecting abnormal changes of volume strainmeter data (in Japanese with English abstract). *Quart. J. Seismol.* **1995**, *59*, 7-29.
13. Kobayashi, A. Detectability of precursory slip expected to occur before the Tokai earthquake as measured by the volumetric strainmeter network (in Japanese with English abstract). *Quart. J. Seismol.* **2000**, *63*, 17-33.
14. Bachmann, C.; Schorlemmer, D.; Woessner, J.; Wiemer, S. Probabilistic estimates of monitoring completeness of seismic networks (abstract), *EOS Trans. Am. Geophys. Un.* **2005**, *86*(52), Fall Meet. Suppl., Abstract S33-0304.
15. Kimura, H.; Miyaoka, K. Observation of short-term slow slip events in Tokai area by strainmeter (in Japanese), *2017 Seismol. Soc. Japan Fall Meet.* **2017**, S03-P13.
16. Tsuboi, C. Determination of the Gutenberg–Richter's magnitude of shallow earthquakes occurring in and near Japan (in Japanese). *Zisin* **1954**, *7*, 185–193.
17. Scordilis, E. M. Globally valid relations converting M_s , m_b and M_{JMA} to M_W , in Book of Abstracts of NATO Advanced Research Workshop, Earthquake Monitoring and Seismic Hazard Mitigation in Balkan Countries (Borovetz, Bulgaria, September 11 – 17, 2005), edited by E. S. Husebye and C. Christova, pp. 158–161, Kamea Ltd., Sofia.
18. Japan Meteorological Agency. Revision of JMA magnitude (in Japanese). *Newslett. Seismol. Soc. Japan* **2003**, *15*(3), 5–9.
19. Baba, T.; Tanioka, Y.; Cummins, P.R.; Uhira, K. The slip distribution of the 1946 Nankai earthquake estimated from tsunami inversion using a new plate model. *Phys. Earth Planet. Inter.* **2002**, *132*, 59–73.
20. Nakajima, J.; Hasegawa, A. Subduction of the Philippine Sea plate beneath southwestern Japan: Slab geometry and its relationship to arc magmatism. *J. Geophys. Res.* **2007**, *112*, B08306.
21. Hirose, F.; Nakajima, J.; Hasegawa, A. Three-dimensional seismic velocity structure and configuration of the Philippine Sea slab in southwestern Japan estimated by double-difference tomography. *J. Geophys. Res.* **2008**, *113*, B09315.
22. Nakajima, J.; Hirose, F.; Hasegawa, A. Seismotectonics beneath the Tokyo metropolitan area, Japan: Effect of slab-slab contact and overlap on seismicity. *J. Geophys. Res.* **2009**, *114*, B08309.
23. Araki E.; Saffer, D.M.; Kopf, A.J.; Wallace, L.M.; Kimura, T.; Machida, Y.; Ide, S.; Davis, E.; IODP Expedition 365 shipboard scientists. Recurring and triggered slow-slip events near the trench at the Nankai Trough subduction megathrust. *Science* **2017**, *356*(6343), 1157-1160.
24. Sato, Y. Crustal deformation associated with the 1944 Tonankai earthquake (in Japanese). *J. Geod. Soc. Japan* **1970**, *15*(4), 177-180.
25. Mogi, K. Temporal variation of crustal deformation during the days preceding a thrust-type great earthquake -The 1944 Tonankai earthquake of magnitude 8.1, Japan. *Pure Appl. Geophys.* **1984**, *122*(6), 765–780.
26. Wyatt, F.K. Measurements of coseismic deformation in southern California: 1972–1982. *J. Geophys. Res.* **1988**, *93*, 7923–7942.
27. Kanamori, H. Initiation process of earthquakes and its implications for seismic hazard reduction strategy. *Proc. Nat. Acad. Sci.* **1996**, *93*, 3726-3731.
28. Scholz, C.; Molnar, P.; Johnson, T. Detailed studies of frictional sliding of granite and implications for the earthquake mechanism. *J. Geophys. Res.* **1972**, *77*, 6392-6406.
29. Lorenzetti, E.; Tullis, T.E. Geodetic predictions of a strike-slip fault model: Implications for intermediate- and short-term earthquake prediction. *J. Geophys. Res.* **1989**, *94*, 12343-12361.

30. Kato, N.; Hirasawa, T. Forecasting aseismic slips and crustal deformation preceding the anticipated Tokai earthquake (in Japanese). *Chikyu monthly* **1996**, *14*, 126-132.
31. Miyaoka, K.; Kimura, H. Detection of long-term slow slip event by strainmeters using the stacking method (in Japanese with English abstract). *Quart. J. Seismol.* **2016**, *79*, 15-23.
32. Cabinet Office Government of Japan (in Japanese). http://www.bousai.go.jp/jishin/nankai/tyosabukai_wg/ (accessed on 11 March 2019).
33. Kanamori, H. Tectonic implications of the 1944 Tonankai and the 1946 Nankaido earthquakes. *Phys. Earth Planet. Inter.* **1972**, *5*, 129-139.
34. Ando, M. Source mechanism and tectonic significance of historical earthquakes along the Nankai Trough, Japan. *Tectonophysics* **1975**, *27*, 119-140.
35. Ishibashi, K. Status of historical seismology in Japan. *Ann. Geophys.* **2004**, *47*, 339-368.
36. Nanjo K.Z.; Yoshida, A. A *b* map implying the first eastern rupture of the Nankai Trough earthquakes. *Nat. Commun.* **2018**, *9*, 1117.
37. Central Disaster Management Council of the Japanese Government (in Japanese). <http://www.bousai.go.jp/jishin/nankai/index.html> (accessed on 11 March 2019).
38. Wessel, P.; Smith, W.H.F.; Scharroo, R.; Luis, J.F.; Wobbe, F. Generic Mapping Tools: improved version released. *EOS Trans. AGU* **2013**, *94*, 409-410.
39. Working Group on Forecast Ability of Large Earthquakes in the Nankai Trough (September 2016 – July 2017) (in Japanese). http://www.bousai.go.jp/jishin/nankai/tyosabukai_wg/ (accessed on 11 March 2019).